Application of theoretical modeling to multichannel active control of cooling fan noise[a)]

Kent L. Gee[b)] and Scott D. Sommerfeldt
Department of Physics and Astronomy, N-283 ESC Brigham Young University, Provo, Utah 84602

(Received 3 April 2003; revised 11 October 2003; accepted 20 October 2003)

Multichannel active control has been applied to the global reduction of tonal noise from a cooling fan. In order to achieve consistent far-field attenuation of multiple harmonics of the blade passage frequency (BPF) of the fan, an analytical model has been applied to the control system in order to determine appropriate transducer configurations. The results of the modeling show that the additional global reduction possible by locating acoustically compact secondary sources coplanar with a compact primary source rapidly lessens as the number of symmetrically placed sources is increased beyond three. Furthermore, the model suggests that there are locations in the extreme near field of the sources that can be considered ideal for the minimization of far-field radiated power. Experiments carried out show that a four-channel control system is more effective than a two-channel system at achieving far-field attenuations, especially at the higher harmonics of the BPF for the fan tested. In addition, greater far-field mean-square pressure attenuations are achieved with the error microphones located along the calculated ideal regions than for nonideal placement.
 [DOI: 10.1121/1.1631940]

PACS numbers: 43.50.Ki [KAC] Pages: 228–236

I. INTRODUCTION

Fan noise has been a widely researched application of active noise control (ANC) since the development of adequate digital signal processing technology. Although the vast majority of investigations has been directed toward ducted fans,[1–4] such as turbofans,[2–4] a small number of studies has been carried out on the reduction of radiated tonal noise from the axial flow fans used to cool electronic devices.[5–7] Single-channel efforts, by Quinlan,[5] Lauchle *et al.*,[6] and Wu,[7] have shown that active control is indeed a viable method of reducing harmonics of the blade passage frequency (BPF), which typically dominate the overall spectrum. However, at the same time, the research carried out previously has suggested the need for further study. Two specific improvements that are examined in this paper are to (1) increase global reductions of the first four harmonics of the BPF by using a multichannel control system, and (2) increase practicality of the ANC system by locating error sensors in the near field of the fan. Because near-field placement of error sensors while seeking far-field attenuation has been deemed ''risky'' by Hansen and colleagues,[8,9] an optimization technique is needed to select an appropriate control actuator arrangement and then to ensure the sensors' locations result in consistent far-field reductions for that actuator configuration.

Performance optimization of an ANC system depends on a number of factors, including the characteristics of the primary noise source, noise environment, and performance criteria. A number of studies have been performed with regards to the maximization of global ANC in a variety of contexts. While the majority of adaptive active control schemes have sought to minimize squared pressure using a form of the filtered-*x* algorithm, other methods have been studied. In some situations, a cost function based on energy density[10] or mean active intensity[8] has been found to be superior to the squared pressure cost function. Much of the research aimed at optimizing transducer configurations has primarily dealt with the reduction of structural acoustic radiation,[11–13] and, more specifically, the noise generated by extended radiators such as electrical transformers.[14,15] Because a small cooling fan represents a significantly different noise source, much of the research has not been found to be extremely applicable and therefore is only briefly summarized where appropriate.

The research regarding the role of transducers in ANC can be largely grouped in two categories, namely investigations involving control actuators and error sensors. Nelson *et al.*[16] described the minimum power output for various configurations of free-field point sources, thereby showing the maximum sound power attenuation possible for similar configurations consisting of real monopole-type primary and secondary sources. Martin and Roure modeled the primary source field using a spherical harmonic multipole expansion in order to determine the optimal location for control sources.[14,17] Others have also examined the use of multipoles as control sources because significant global far-field attenuation may still be achieved with a primary source and secondary multipole located at a relatively large fraction of a wavelength from each other.[18–20]

The optimization of error sensing techniques has also received considerable attention. A number of near-field error sensing schemes has been theoretically examined by Qiu *et al.*[8] Despite their finding that minimization of the mean active intensity normal to a surface surrounding all sources is

[a)]Portions of this work were presented in ''Multi-channel active control of cooling fan noise,'' *143rd Meeting: Acoustical Society of America*, Pittsburgh, PA, June 2002, and ''Multichannel active control of cooling fan noise,'' *Proceedings of Inter-Noise 2002*, Dearborn, MI, August 2002.

[b)]Graduate Program in Acoustics, Pennsylvania State University, P.O. Box 30, State College, PA 16804. Electronic mail: kentgee@psu.edu

the ideal near-field sensing strategy, Berry, *et al.*[12] compared the minimization of intensity versus squared pressure for a vibrating plate and found that intensity minimization provided negligible improvement over near-field squared pressure minimization. Also, Wang[13] and Martin and Roure[17] made use of genetic search algorithms in order to determine the optimal locations for farfield error microphone locations.

In this paper, we discuss a modeling technique based on the work of Nelson *et al.*[16] is discussed which is used to both determine an appropriate configuration of control sources and to suggest near-field error microphone locations that result in consistent far-field reductions for multiple harmonics of the BPF radiated from a small cooling fan. Following a description of the modeling performed, experimental results are presented and analyzed.

II. THEORETICAL MODELING

A. Source modeling

1. Primary source

Before the development of an appropriate method to determine control system transducer locations, it is necessary to first discuss the disturbance noise source itself. The spectrum of a cooling fan consists of a broadband component upon which is superimposed one or more discrete-frequency peaks, which are harmonically related to the BPF. The dominant noise generation mechanism for the tonal noise with subsonic blade tip speeds is spatially unsteady loading on the fan blades.[21] Unsteady loading may be attributed to flow obstructions near the inlet or exhaust of the fan, such as fan support struts or finger guards.[22] These fluctuating lift and drag forces on the blades generate dipole-like noise. If the tonal frequency and fan diameter are such that the fan may be considered aeroacoustically compact, then the far-field radiation will be that of a dipole, often skewed, as measurements on unbaffled cooling fans have shown.[5,6] However, with the fan baffled, the radiation is closer to that of a monopole. At higher harmonics of the BPF, where the condition of compactness no longer holds, the far-field radiation pattern becomes increasingly complex and directional. The number of harmonics present, their amplitudes, and directional characteristics will largely depend on the nature of the unsteady loading.

Because the radiation at the BPF is fairly smooth and omnidirectional for the fan and experimental configuration used, the fan is modeled as a point monopole source, mounted in an infinite baffle. Although the experimental fan may not strictly be considered baffled, since it is mounted in an aluminum enclosure roughly the size of a personal computer chassis, the infinite baffle assumption greatly simplifies the calculations. Furthermore, even though the fan's radiation becomes more complex as a function of frequency, the decreasing wavelength causes the fan to appear more baffled at higher harmonics of the BPF. Because of this, the radiation of the fan is modeled as a monopole source up to the fourth harmonic of the BPF, which is the highest tone targeted by the ANC system.

2. Control sources

A practical ANC system that could be applied to typical commercial cooling fan applications (e.g., a personal computer) would have to be compact and self-contained, that is to say, the actuators and sensors would need to be mounted in or on the device. It is necessary, therefore, to determine actuator and sensor locations in the near field of the fan that lead to global far-field reductions. Because the fan is assumed to be baffled, the secondary sources will be located on the baffle. Furthermore, although the use of multipoles as control sources has been found to be advantageous in some instances,[14,17–20] the requirement of system compactness precludes the use of these types of actuators. Finally, because the loudspeakers used in this investigation as control actuators have a smaller diameter than the fan and can be considered more acoustically compact over the frequency range of interest, they are also modeled as point monopoles.

B. Determination of control source configurations

With the fan and ANC system actuators modeled as point monopole sources, an analysis similar to that of Nelson *et al.* can be performed in order to discover an appropriate configuration for control sources. The purpose of the approach is to determine the minimum power radiated by a given control source configuration. By examining various control source arrangements, the optimal configuration can then be determined. The procedure for finding the minimum radiated power for a system of point sources is well documented in Refs. 16 and 23, and therefore is briefly summarized as follows. First, control source locations are determined and the sources given arbitrary complex strengths relative to that of the primary source. Second, because the mutual acoustic coupling of multiple point sources is well understood analytically, a mathematical expression for the radiated power from all sources may then be obtained. Third, the source strengths that minimize the total radiated power may be obtained by differentiating the total radiated power expression with respect to the real and imaginary parts of each of the control source strengths, setting each resultant equation equal to zero, and solving for the optimal strengths. Other than the baffled source assumption, the analysis is only different from that of Nelson *et al.*, in the sense that all sources are required to be located in the same plane, a restriction not imposed by the previous research. The fact that the sources are baffled only scales all source strengths by a factor of 2; the relative strengths of primary and secondary sources and radiated power are identical to the unbaffled case.

The source strength optimization technique has been carried out for a number of configurations not included in the Nelson *et al.* analysis.[24] Two such configurations, that of four and eight secondary sources arranged symmetrically around and in the same plane as the primary source, are displayed schematically after the manner of Nelson and colleagues in Fig. 1. The minimum radiated power, relative to the primary source alone, is shown in Fig. 2 as a function of *kd*, which is the nondimensionalized separation distance between the primary and secondary sources. Displayed is the radiated power

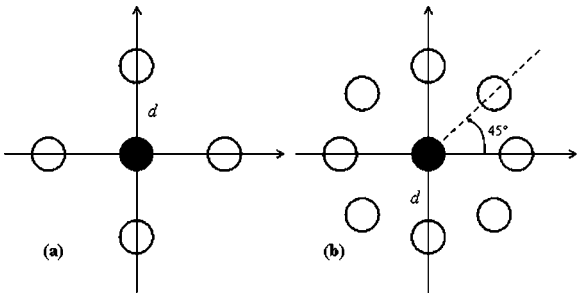

FIG. 1. Point source monopole configurations, after the manner of those shown by Nelson *et al.* in Fig. 5 of Ref. 16. The primary source (shaded) is located at the origin. Configuration (a) consists of four secondary sources, each at a distance, *d*, from the primary source and placed at 90° increments. Arrangement (b) contains eight secondary sources, each at a distance, *d*, from the primary source and are each separated by 45° angles.

for the configurations analyzed previously by Nelson *et al.*,[16] denoted by (N) in the figure legend, as well as for the source arrangements in Fig. 1. The source configuration that yields the most attenuation for a separation distance of less than a half-wavelength ($kd<\pi$) is the tetrahedral arrangement shown in Fig. 5(c) of Ref. 16, in which the primary source is at the center of the tetrahedron and equidistant from all four secondary sources. While this is not a valid arrangement under the imposed limitation that all sources be located in the same plane, it does demonstrate that greater suppression of power radiated from the primary source can be achieved with a three-dimensional source arrangement.

An examination of the five source configurations in which the limitation is met yields another important result: the additional reduction that can be achieved as more sources are added and symmetry is maintained rapidly lessens. As *kd* becomes small, three, four, and eight symmetrically arranged and optimized secondary sources provide essentially the same power reduction. While the greatest difference between the three and four secondary source arrangements for $kd<\pi$ is on the order of 1 dB, the largest difference between four and eight sources over the same range is less than 0.2 dB. For $kd>\pi$, even though the overall reduction possible for any configuration is small, it is interesting to note that for the range shown, the reduction in radiated power for the tetrahedral distribution is actually less than that of the four and eight coplanar source arrangements. However, because of the desire to locate the primary and control sources as close as possible, this latter result is considered secondary. The power-minimization results for the planar configurations described suggest that either three or four monopole-like actuators placed symmetrically around the fan is a practical limit to optimize global control of a baffled compact source.

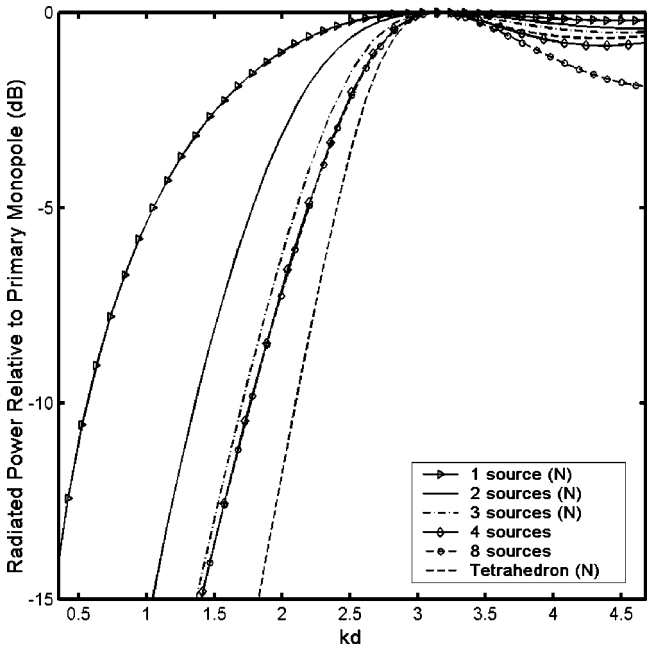

FIG. 2. Radiated power, relative to that radiated by the primary monopole itself, for secondary source arrangements. The secondary source strengths have been chosen so as to minimize the radiated power of the system. Those configurations marked by an (N) in the figure legend have been analyzed previously by Nelson *et al.* in Ref. 16. The other two arrangements are those depicted in Fig. 1.

C. Determination of near-field error sensor locations

The preceding analysis does not include the determination of error sensor locations that result in global control, which is a necessary step in developing a viable, robust ANC system. For this particular application, the issue is complicated by the requirement that the error sensors be located in the near field, yet yield far-field reductions. Near-field error sensor placement has been traditionally warned against, in that sound power attenuation can vary rapidly as a function of location[9] and far-field pressure reductions may be accompanied by pressure increases in the near field.[8] The subsequent discussion describes the determination of appropriate near-field error sensor locations based on a continuation of the analysis performed in the previous section.

For the active control of free-field radiation, the optimal error sensor locations are those where the acoustic pressure attenuation is greatest when the control sources' strengths are such that the overall power radiated is minimized.[9] Error sensors may then be suitably located in the near field by discovering the point or regions of greatest pressure attenuation. The method of locating these regions used in this investigation is that of plotting the two-dimensional magnitude of the near-field pressure attenuation in the plane of the sources for the condition of minimized power radiation, and then determining an appropriate location graphically. An alternative to the graphical method would be to develop an analytical expression for optimal placement as a function of frequency and position relative to the primary source, however, this approach was not utilized for two reasons. First, just as the fan and control loudspeakers are not point sources, the error sensors used in practice are not point sensors, but microphones with diaphragms of finite width, and therefore it would likely be pointless to attempt to ascertain with extreme precision the optimal locations. Second, it may be shown that some of the points considered ideal are so close to the primary source that, in practice, noise induced by the airflow across the microphones due to the fan results in a poor signal-to-noise ratio. For these reasons, the graphical method has been chosen as a guide for approximate near-field error microphone placement.

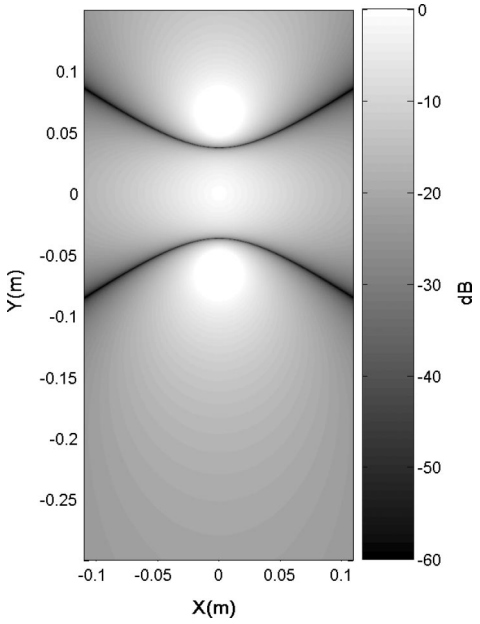

FIG. 3. The magnitude of the radiated pressure, relative to that of the primary source by itself, at 370 Hz (1×BPF) along the dimensions of the experimental enclosure for two optimized secondary monopoles located at (0,0.06) and (0,−0.06) m and the primary source located at the origin. The regions for optimal error sensor placement are demarcated by the pressure nulls.

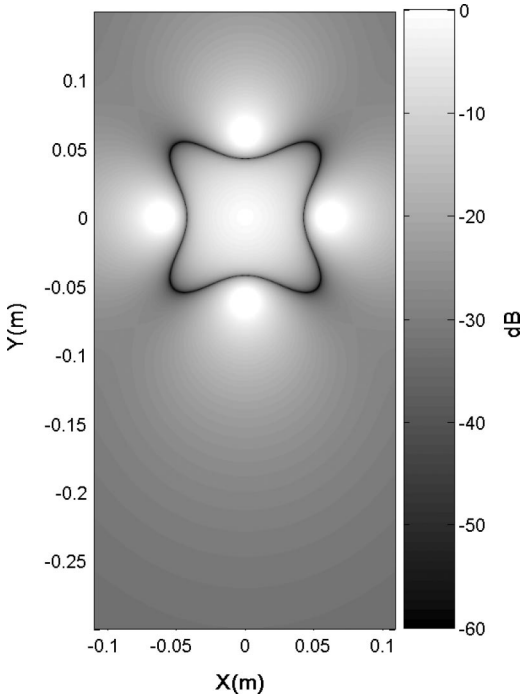

FIG. 4. The magnitude of the radiated pressure, relative to that of the primary source by itself, at 370 Hz (1×BPF) along the dimensions of the experimental enclosure for four optimized secondary monopoles located at (0.06,0), (0,0.06), (−0.06,0), and (0,−0.06) m. The primary source is located at the origin.

Although other control configurations have been studied both theoretically and experimentally,[24,25] the effect of error sensor location on global reductions for two source arrangements has received particular experimental focus. These configurations are that of the two sources, placed on opposite sides of the primary source, as discussed by Nelson *et al.*, and the four sources located symmetrically around the primary source. The magnitude of the near-field pressure, normalized by the pressure of the primary source by itself, for these two configurations is plotted in Figs. 3–5, for the dimensions of the enclosure face on which the control sources are located. For these figures, the control source strengths have been set so as to minimize the overall radiated power. The distance between the primary source located at the origin and the secondary sources is 0.06 m. Figures 3 and 4 display the pressure magnitude for 370 Hz, the BPF of the fan used in the experiments, for the two and four control source arrangements, respectively. It is clearly seen from these two plots of the near-field pressure that nulls exist in the radiation pattern when the control sources radiate in the minimized-power state. Because the pressure attenuation is the greatest in these regions, the ideal error sensor locations are delimited by the nulls. In the case of the two control source configuration, the two nulls that curve between the primary and secondary sources continue out to the far-field, approaching asymptotes that pass through the origin. The slope of these asymptotes gradually lessens as frequency increases; however, over the range plotted the arclength is small enough that the locations of the nulls remain fairly constant for the first four harmonics of the BPF.

The near-field pressure null for the four source configuration demonstrates markedly different behavior than those of the previous analysis. Instead of continuing out to the far-field, the null is of closed form and only exists in the near field. The frequency dependence of the null location is shown by comparing Figs. 4 and 5, the latter of which shows the near-field pressure attenuation at the fourth harmonic of

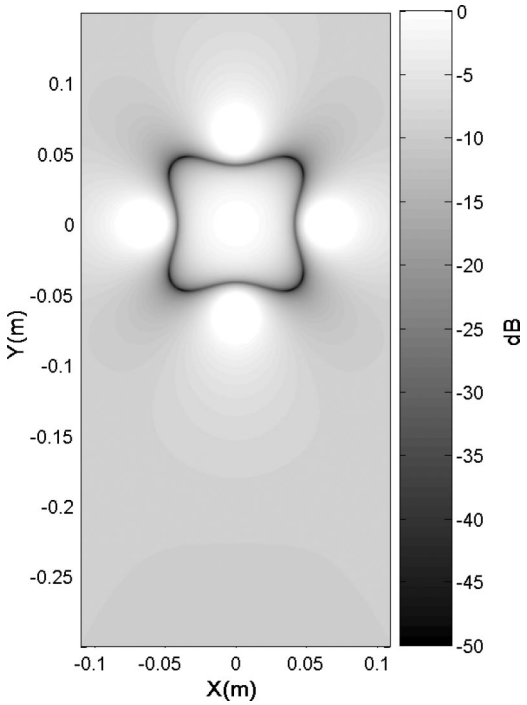

FIG. 5. The magnitude of the radiated pressure, relative to that of the primary source by itself, at 1480 Hz (4×BPF) for the same four optimized sources as in Fig. 4, showing the changed shape in the near-field null at 45° angles relative to the location of the secondary sources.

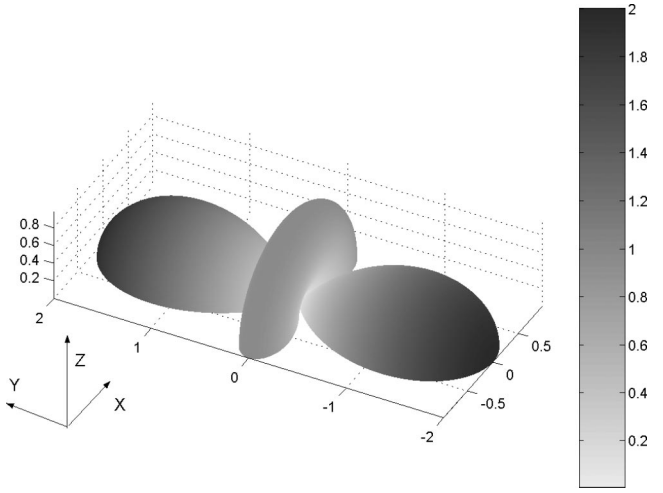

FIG. 6. Linear three-dimensional directivity at 370 Hz for the system with two optimized secondary sources described in Fig. 3. Symmetry of the radiation about the *y* axis signifies that the plane of the sources may be considered an ideal location for error sensors, because there is no dependence on the polar angle, θ.

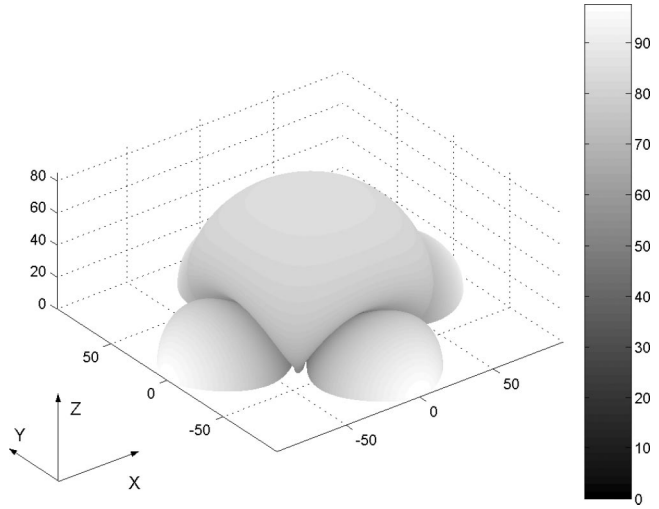

FIG. 7. Three-dimensional directivity, represented logarithmically in dB, at 370 Hz and $r=0.072$ m for the control configuration with four optimized secondary sources described in Fig. 4. The radiation is not symmetric about any of the three Cartesian axes in this case, demonstrating that the near-field null location is a function of both the azimuthal angle, ϕ, and the polar angle, θ.

the BPF, which is 1480 Hz. Like the two control source case, the dependence of the null location on frequency is not extreme, but it does suggest that an appropriate compromise would be to locate an error sensor closer to a control source rather than equidistant between two control sources, where the null location change is the greatest. This technique clearly demarcates appropriate near-field error sensor locations that should allow the control sources to operate under optimal source strength conditions, and therefore lead to maximum far-field attenuations.

D. Justification of error microphone placement in source plane

Before proceeding to an experimental verification of this technique for the two configurations analyzed, it is important to justify placement of the error sensors in the source plane, rather than off the plane. After all, it was shown in the previous section that to begin to truly maximize the reduction of far-field power for $kd<\pi$, a three-dimensional distribution of secondary sources is needed (e.g., the tetrahedral configuration of Nelson *et al.*). This justification of error sensor placement may be expressed as a need to determine the behavior of the pressure attenuation off the source plane to see if the nulls are perhaps deeper than in the plane of the sources. For the two control source case, it can be seen from the directivity plot in Fig. 6 that the pressure radiated from the system of sources is symmetric about the *y* axis. It is then clear that placement of the error sensors in the plane of the sources (the *x*-*y* plane in Fig. 6) may be considered ideal for this configuration. However, for the four control source case, the radiation is not axisymmetric, as can be easily seen in Fig. 7, which shows the directivity of the radiation for 370 Hz at a distance $r=0.072$ m from the primary source. The distance has been chosen on the basis that the three-dimensional directivity will include the near-field null at a number of locations in the plane of the sources, providing the opportunity to observe the behavior of the nulls off the plane.

The pressure directivity for the optimized four control source configuration as a function of azimuthal angle, ϕ, and polar angle, θ, is displayed in Fig. 8. The polar angle, θ, is measured from the axis perpendicular to the source plane, and the azimuthal angle, ϕ, is measured from the *x* axis, shown in Figs. 3–7. The directivity shows that the depth of the null is constant as θ, which is equal to $\pi/2$ in the plane of the sources (i.e., $z=0$), is lessened. This behavior of the null demonstrates that the plane of the sources may also be considered ideal for the placement of error sensors. This same behavior has been verified for various near-field radii (r) and frequencies and is found to be consistent as long as r is such that it includes the near-field null. If error sensors are to be placed anywhere beyond the null, it may also be shown that

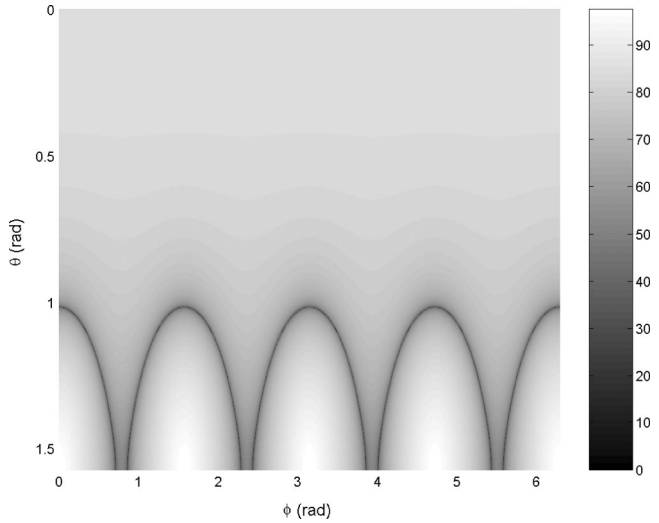

FIG. 8. A two-dimensional representation of Fig. 7, with the polar angle, θ, on the vertical axis and the azimuthal angle, ϕ, on the horizontal axis, showing the behavior of the pressure nulls off the source plane, where $\theta=\pi/2$.

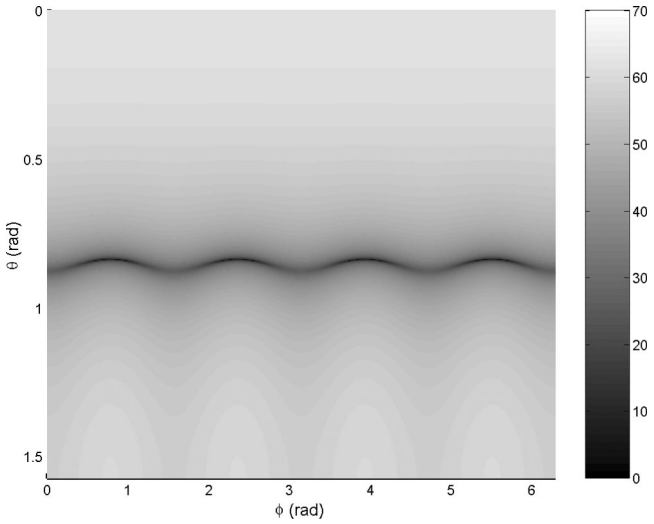

FIG. 9. Two-dimensional representation of the directivity at $r=1.0$ m and a frequency of 1480 Hz for the four secondary source arrangement, demonstrating that the source plane may no longer be considered an ideal location for error sensors.

the greatest areas of pressure attenuation are not found in the source plane, but above it (for example, see Fig. 9).

III. EXPERIMENTAL SETUP

The results of the theoretical modeling carried out indicate that there are appropriate near-field error sensor locations for the two and four control actuator configurations. These configurations are now examined experimentally. Although Ref. 25, which comprises a parallel investigation on the practical aspects of multichannel ANC of cooling fan noise, contains a more complete description of the experimental apparatus used, the major components are summarized here.

The cooling fan used is a seven-bladed, 80 mm DC Mechatronics fan, which has been housed in a $9.5\times18\times16$ in. ($0.24\times0.46\times0.41$ m) aluminum enclosure intended to simulate a desktop computer tower or server chassis. A one inch wide rectangular obstruction has been mounted on the inlet side of the fan to create a time-invariant flow distortion. Four 1-1/8 in. (0.029 m) diameter Radio Shack loudspeakers surround the fan such that they are equidistant from each other and the distance between the center of the fan and the center of each loudspeaker is 0.06 m. The reference signal, which is required in the single reference, multiple output adaptive filtered-*x* controller, is supplied by locating a small infrared LED on the inlet of the fan and a matched phototransistor detector on the exhaust side of the fan, such that the blades passing between them creates a pseudosquare pulse train whose period corresponds to the BPF. Larson Davis Type-I microphones are mounted on the surface of the aluminum enclosure for error sensing and additional microphones are mounted on a rotatable semicircular measurement boom of radius 5 ft (1.52 m) for global performance monitoring. The 13 boom microphones are placed at equal angles along the boom and can therefore provide an estimate of the global mean-square pressure radiated by the fan at a given frequency.

IV. RESULTS AND DISCUSSION

The results of the theoretical analysis carried out have been utilized in conjunction with the above experimental apparatus to investigate the effect on the global attenuation of the fan by (1) a two-channel versus a four-channel ANC system; and (2) the placement of error microphones in ideal versus nonideal locations. Graphical results from both of the actuator configurations, meant to demonstrate typical reductions achieved with the error microphones located ideally, are first shown. These results are followed by numerical results and a discussion of the mean performance of each of the four configurations.

A. Graphical results

In order to determine the global mean-square pressure reductions achieved by a particular control configuration, a reference pressure measurement without ANC has been taken using the measurement boom. In Figs. 10 and 11, the directivity of the fan without control is represented by a wire frame mesh for each of the four targeted harmonics of the BPF, namely 370, 740, 1110, and 1480 Hz. The fan's radiation pattern becomes more directional and complex with increasing frequency, as the fan becomes less aeroacoustically compact.

Results are displayed in Fig. 10 for the first experimental configuration, a two-channel setup with the loudspeakers located on opposite sides of the fan and along the same axis, as described previously. The test channel count refers to the number of loudspeakers, error microphones, and control signals generated by the adaptive controller. A two-channel configuration will be often referred to hereafter as ''2×2 control.'' For the trial shown in Fig. 10, the reductions in far-field mean-square pressure for the four harmonics of the BPF are 6.6, 9.8, 9.3, and 2.8 dB. The overall A-weighted tonal reduction [*dBAred* in Eq. (1)] is 7.5 dBA, which is calculated according to

$$\mathrm{dBAred}=10\log\left(\frac{\Sigma_{n=1}^{4}{p_{\mathrm{ANC\_OFF}}}^{2}(f_n)A^2(f_n)}{\Sigma_{n=1}^{4}{p_{\mathrm{ANC\_ON}}}^{2}(f_n)A^2(f_n)}\right), \qquad (1)$$

where $p^2(f_n)$ signifies the mean-square pressure for the nth harmonic of the BPF, represented by f_n, and A is the narrowband A-weighting function evaluated at the appropriate frequency. As with virtually all multichannel tests, the second harmonic, shown in Fig. 10(b), is reduced more than the fundamental, which is displayed in Fig. 10(a). In this case, the reduction of the third harmonic is also greater than that of the BPF. This may be attributed to the relatively poor response of the loudspeakers at 370 Hz.[24,25] Attenuation for the fourth harmonic, shown in Fig. 10(d), is much less significant than for the other three harmonics.

The global attenuations for a four-channel (4×4) test, again with the error microphones located ideally, are shown in Fig. 11. The mean-square pressure reductions for the four targeted frequencies are 9.5, 18.5, 14.4, and 7.6 dB, resulting in an overall tonal reduction of 11.4 dBA. Again, the attenuation of the second and third harmonics is greater than that of the fundamental, which may be seen by comparing Figs. 11(a)–11(c). The attenuation of the fourth harmonic, seen in

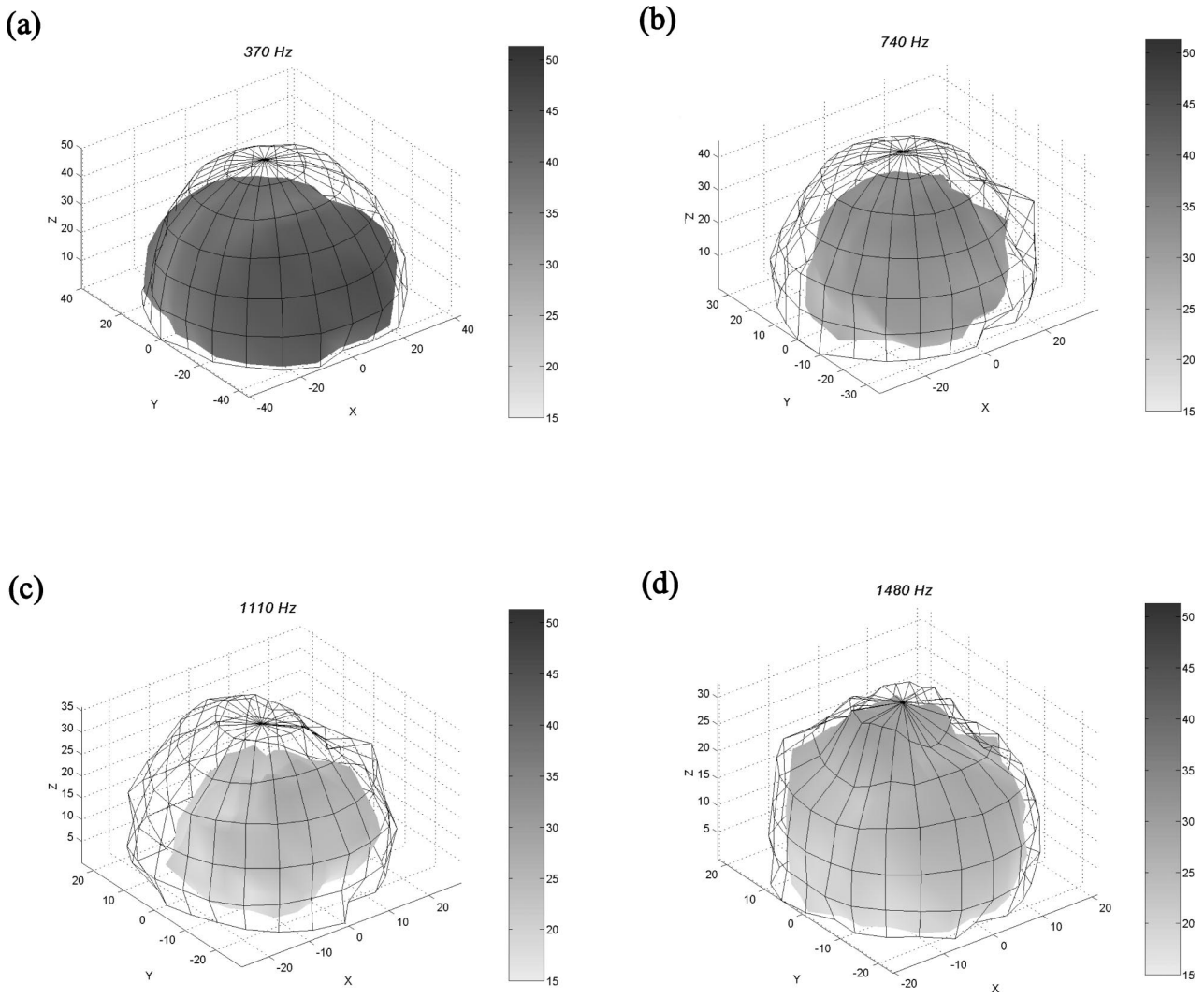

FIG. 10. Directivity of the BPF and harmonics without (mesh) and with (solid surface) two-channel active control, with the error microphones located in a theoretically ideal region. Both the radius from the origin and shading are proportional to the sound pressure level for a given angle.

Fig. 11(d), is only about 2 dB less than that of the fundamental, which again demonstrates the limitations imposed by the loudspeakers on the performance capabilities of the system at low frequencies.

B. Numerical results

The results displayed in the previous section are useful in understanding the capabilities of the multichannel ANC system for a single trial; however, little has been reported in the literature about the mean performance of active control systems. In Ref. 25, however, data are presented that show average mean-square pressure reductions of the tonal noise solely as a function of actuator configuration. Shown in Table I are the results of averaging the mean-square pressure attenuations for 2×2 and 4×4 control, for both the error microphones located along the theoretically ideal regions and also for nonideal placement. The results are obtained by selecting, for each configuration, the eight trials that yield the largest overall A-weighted tonal reductions. It is not possible to consider the mean performance of all trials because some nonideal error microphone locations quickly led to controller instability, and these divergent trials would need to be somehow included in the analysis to yield unbiased results. The results in Table I therefore serve as an average of the maximum mean-square pressure reductions yielded by the four configurations.

C. Discussion

The data in Table I demonstrate that, on the whole, the 4×4 setup provides a greater global attenuation of the fan tones than does the 2×2 configuration, corroborating the results of Ref. 25. In addition, placement of the error microphones along the theoretical nulls results in greater overall A-weighted tonal attenuations for both the two- and four-channel systems, although for the 2×2 arrangement, the nonideal locations yield greater mean-square pressure reductions for the third and fourth harmonics. While the tabular data serves to show quantitatively that greater reductions are possible with the error microphones located along the regions calculated to be theoretically ideal, some other qualitative observations are also worthwhile regarding system behavior as a function of error microphone placement.

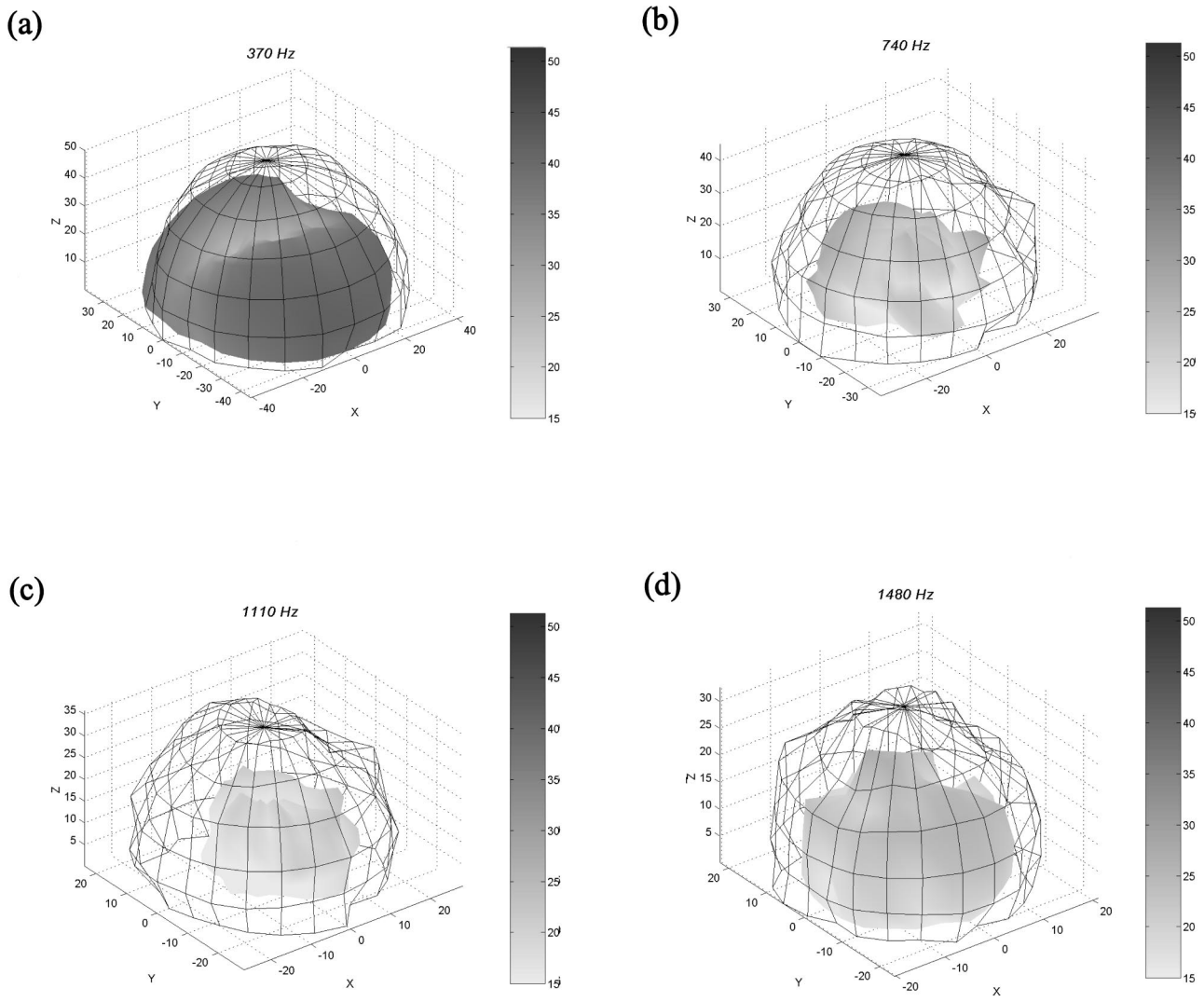

FIG. 11. Directivity of the BPF and harmonics without (mesh) and with (solid surface) four-channel active control, with the error microphones located in a theoretically ideal region. Both the radius from the origin and shading are proportional to the sound pressure level for a given angle.

Some comments with regards to controller stability, although qualitative in nature, help in fully describing the effect of error microphone placement on global tonal attenuations. Placement of the error microphones in locations determined to be theoretically ideal tends to result in control signals with smaller amplitudes and therefore a more stable controller; the adaptive controller very rarely diverges with the error microphones located ideally. However, nonideal (e.g., random) placement of the error microphones often produces large control signals and loudspeaker distortion, ultimately leading to positive feedback and divergence of the control system. This is especially true of the 4×4 system, whereas the 2×2 system tends to be more stable under loudspeaker distortion, but often yields net global increases in the mean-square pressure rather than attenuations. These results corroborate the findings of Baek and Elliott, which state that transducer positions resulting in low control effort are good choices when robust control is desired.[26]

TABLE I. Mean-square pressure reduction (MPR) and standard deviation (σ), in dB, averaged over the eight best trials for each type of configuration. ''Ideal'' signifies the error microphones are located along the theoretical nulls; ''nonideal'' means the error microphones are located somewhere off the nulls. Results for the first four harmonics of the BPF and the overall A-weighted tonal levels are shown.

	370 Hz		740 Hz		1110 Hz		1480 Hz		A-weighted Total	
All results in dB	MPR	σ	MPR	σ	MPR	σ	MPR	σ	MPR	σ
2×2 nonideal	5.3	2.5	10.9	5.0	6.9	3.9	4.2	2.5	6.5	2.7
2×2 ideal	8.4	2.5	11.9	3.1	5.9	2.7	3.1	3.0	8.0	1.2
4×4 nonideal	8.2	1.6	14.9	3.4	11.0	3.9	7.4	4.1	9.5	1.5
4×4 ideal	10.1	1.0	16.1	2.1	12.8	2.4	8.7	3.5	11.4	0.4

V. CONCLUSIONS

A theoretical modeling technique based on the previous work of Nelson *et al.*[16] has been applied to the multichannel active control of a small axial cooling fan. All sources have been represented as baffled ideal point sources and the control source strengths that minimize the overall radiated power have been found for various configurations. An examination of the radiated power as a function of nondimensional source separation distance shows that, under the restriction that all sources be coplanar and closely located, the amount of additional sound power reduction possible rapidly lessens as the number of symmetrically placed control sources is increased beyond three. This result suggests that a practical limit to the necessary number of symmetric control sources to maximize global attenuations from an acoustically compact coplanar noise source is three or four, depending on the frequency content of the primary source radiation. Moreover, for a given idealized point source configuration possessing relative source strengths such that the radiated power is minimized, an analysis of the radiated pressure in the plane of the sources has led to the discovery of ideal near-field error microphone locations.

These error microphone locations have been experimentally examined for two-channel and four-channel configurations and results describing the mean optimum performance of the active control system show that greater overall reductions may be achieved with the error microphones located in the theoretically ideal regions, rather than nonideal or random locations. Furthermore, ideal placement of the error microphones appears to lead to a more stable control environment, whereas random placement of the microphones often contributes to controller instability due to a large control effort and subsequent loudspeaker distortion. The results of this investigation show that significant global reductions of four harmonics of the BPF may be achieved upon utilization of an idealized model of the sources, and that the near-field placement of error microphones is plausible for global active control of the radiation from compact sources.

[1] G. H. Koopmann, D. J. Fox, and W. Neise, ''Active source cancellation of the blade tone fundamental and harmonics in centrifugal fans,'' J. Sound Vib. **126**, 209–220 (1988).

[2] R. H. Thomas, R. A. Burdisso, C. R. Fuller, and W. F. O'Brien, ''Active control of fan noise from a turbofan engine,'' AIAA J. **32**, 23–30 (1994).

[3] C. H. Gerhold, ''Active control of fan-generated tone noise,'' AIAA J. **37**, 17–22 (1997).

[4] R. Kraft, Z. Hu, S. Sommerfeldt, B. Walker, A. Hersh, H. Jo, M. Spencer, D. Hallman, C. Mitchell, and D. Sutliff, ''Development and demonstration of active noise control concepts,'' NASA CR-2000-210037, 2000.

[5] D. A. Quinlan, ''Application of active control to axial flow fans,'' Noise Control Eng. J. **101**, 95–101 (1992).

[6] G. C. Lauchle, J. R. MacGillivray, and D. C. Swanson, ''Active control of axial-flow fan noise,'' J. Acoust. Soc. Am. **101**, 341–349 (1997).

[7] M. Q. Wu, ''Active cancellation of small cooling fan noise from office equipment,'' *Proceedings of Inter-Noise 95*, Newport Beach, CA (Noise Control Foundation, Poughkeepsie, NY, 1995), pp. 525–528.

[8] X. Qiu, C. H. Hansen, and X. Li, ''A comparison of near-field acoustic error sensing strategies for the active control of harmonic free field sound radiation,'' J. Sound Vib. **215**, 81–103 (1998).

[9] C. H. Hansen and S. D. Snyder, *Active Control of Noise and Vibration* (E & FN SPON, London, 1997).

[10] J. W. Parkins, S. D. Sommerfeldt, and J. Tichy, ''Narrowband and broadband active control in an enclosure using the acoustic energy density,'' J. Acoust. Soc. Am. **108**, 192–203 (2000).

[11] R. L. Clark and C. R. Fuller, ''Optimal placement of piezoelectric actuators and polyvinylidene fluoride error sensors in active structural acoustic control,'' J. Acoust. Soc. Am. **92**, 1521–1533 (1992).

[12] A. Berry, X. Qiu, and C. H. Hansen, ''Near-field sensing strategies for the active control of the sound radiated from a plate,'' J. Acoust. Soc. Am. **106**, 3394–3406 (1999).

[13] B.-T. Wang, ''Optimal placement of microphones and piezoelectric transducer actuators for far-field sound radiation control,'' J. Acoust. Soc. Am. **99**, 2975–2984 (1996).

[14] T. Martin and A. Roure, ''Active noise control of acoustic sources using spherical harmonics expansion and a genetic algorithm: Simulation and experiment,'' J. Sound Vib. **212**, 511–523 (1998).

[15] K. A. Cunefare and G. H. Koopmann, ''Global optimum active noise control: Surface and far-field effects,'' J. Acoust. Soc. Am. **90**, 365–373 (1991).

[16] P. A. Nelson, A. R. D. Curtis, S. J. Elliott, and A. J. Bullmore, ''The minimum power output of free field point sources and the active control of sound,'' J. Sound Vib. **116**, 397–414 (1987).

[17] T. Martin and A. Roure, ''Optimization of an active noise control system using spherical harmonics expansion of the primary field,'' J. Sound Vib. **201**, 577–593 (1997).

[18] J. S. Bolton, B. K. Gardner, and T. A. Beauvilain, ''Sound cancellation by the use of secondary multipoles,'' J. Acoust. Soc. Am. **98**, 2343–2362 (1995).

[19] T. A. Beauvilain, J. S. Bolton, and B. K. Gardner, ''Sound cancellation by the use of secondary multipoles: Experiments,'' J. Acoust. Soc. Am. **107**, 1189–1202 (2000).

[20] X. Qiu and C. H. Hansen, ''Secondary acoustic source types for active noise control in free field: Monopoles or multipoles?,'' J. Sound Vib. **232**, 1005–1009 (2000).

[21] W.-S. Chiu, G. C. Lauchle, and D. E. Thompson, ''Subsonic axial flow fan noise and unsteady rotor force,'' J. Acoust. Soc. Am. **85**, 641–647 (1989).

[22] K. B. Washburn and G. C. Lauchle, ''Inlet flow conditions and tonal sound radiation from a subsonic fan,'' Noise Control Eng. J. **31**, 101–110 (1988).

[23] P. A. Nelson and S. J. Elliott, *Active Control of Sound* (Academic, London, 1992).

[24] K. L. Gee, ''Multi-channel active control of axial cooling fan noise,'' MS thesis, Brigham Young University, Provo, UT, 2002.

[25] K. L. Gee and S. D. Sommerfeldt, ''A compact active control implementation for axial cooling fan noise,'' Noise Control Eng. J., accepted for publication.

[26] K. H. Baek and S. J. Elliott, ''The effects of plant and disturbance uncertainties in active control systems on the placement of transducers,'' J. Sound Vib. **230**, 261–289 (2000).